

# *Reduced-order dynamics of the Martian atmospheric dynamics*

Conference or Workshop Item

Published Version

Martinez-Alvarado, O. ORCID: <https://orcid.org/0000-0002-5285-0379>, Moroz, I. M., Read, P. L. and Lewis, S. R. (2005) Reduced-order dynamics of the Martian atmospheric dynamics. In: 5th EUROMECH Nonlinear Oscillations Conference ENOC-2005, 7 August 2005 - 12 August 2005, Eindhoven, The Netherlands. Available at <https://centaur.reading.ac.uk/36299/>

It is advisable to refer to the publisher's version if you intend to cite from the work. See [Guidance on citing](#).

All outputs in CentAUR are protected by Intellectual Property Rights law, including copyright law. Copyright and IPR is retained by the creators or other copyright holders. Terms and conditions for use of this material are defined in the [End User Agreement](#).

[www.reading.ac.uk/centaur](http://www.reading.ac.uk/centaur)

**CentAUR**

Central Archive at the University of Reading

Reading's research outputs online

## REDUCED-ORDER MODELS OF THE MARTIAN ATMOSPHERIC DYNAMICS

**Oscar Martinez-Alvarado**

Mathematical Institute  
University of Oxford  
24-29 St Giles'  
Oxford, OX1 3DW, UK  
martine2@maths.ox.ac.uk

**Irene M. Moroz**

Mathematical Institute  
University of Oxford  
24-29 St Giles'  
Oxford, OX1 3DW, UK  
moroz@maths.ox.ac.uk

**Peter L. Read**

Department of Physics  
University of Oxford  
Clarendon Laboratory  
Oxford, OX1 3PU, UK  
p.read1@physics.ox.ac.uk

**Stephen R. Lewis**

Department of Physics  
University of Oxford  
Clarendon Laboratory  
Oxford, OX1 3PU, UK  
s.lewis1@physics.ox.ac.uk

### Abstract

In this paper we explore the possibility of deriving low-dimensional models of the dynamics of the Martian atmosphere. The analysis consists of a Proper Orthogonal Decomposition (POD) of the atmospheric streamfunction after first decomposing the vertical structure with a set of eigenmodes. The vertical modes were obtained from the quasi-geostrophic vertical structure equation. The empirical orthogonal functions (EOFs) were optimized to represent the atmospheric total energy. The total energy was used as the criterion to retain those modes with large energy content and discard the rest. The principal components (PCs) were analysed by means of Fourier analysis, so that the dominant frequencies could be identified. It was possible to observe the strong influence of the diurnal cycle and to identify the motion and vacillation of baroclinic waves.

### Key words

Mars, Proper Orthogonal Decomposition, baroclinic waves.

### 1 Introduction

Reduced-order models of the terrestrial atmosphere have been widely studied using the methods of Proper Orthogonal Decomposition (POD) (Achatz and Branstator, 1999; Achatz and Opsteegh, 2003a; Achatz and Opsteegh, 2003b) and Principal Interaction Patterns (PIPs) (Kwasniok, 2004). However, only a few analogous studies have been carried out for extraterrestrial atmospheres (Whitehouse *et al.*, 2004a; White-

house *et al.*, 2004b). Such studies would be invaluable for understanding the long term behaviour of both extraterrestrial and terrestrial atmospheres as an aspect of comparative planetology.

It has been suggested that an important part of the large-scale variability of the dynamics of the Martian atmosphere takes place in a phase space of relatively low dimension (Collins *et al.*, 1996; Read and Lewis, 2004). Whitehouse *et al.* (2004a, 2004b) developed low-order models by means of POD-Galerkin methods for a flat spherical planet whose planetary parameters were chosen to be similar to those of Mars. The relevant physical processes were represented by simple parameterisations such as Newtonian cooling and linear surface drag.

Our aim is to go further and to develop more realistic reduced-order models of the dynamical behaviour of the Martian atmosphere including some relevant physical processes, in particular the interactions with topography and tides. In this paper we shall present results from a diagnostic analysis which suggest that a reduction of the number of dimensions is feasible.

The data to be analysed correspond to a period of 150 sols (1 sol = 1 Martian day, approximately 40 minutes longer than a terrestrial day) during the transition from autumn to winter in the northern Martian hemisphere (1 Martian year = 668.6 sols), when the *baroclinic wave* activity is enhanced, i.e. the development of cyclone-anticyclone systems transporting energy from the equator to the poles is more likely to occur. The data were taken from an assimilation of observations of atmospheric temperatures and dust made by the Thermal Emission Spectrometer (TES) on board of

the Mars Global Surveyor (MGS) into the Oxford Martian General Circulation Model (MGCM). This model solves the *hydrostatic primitive equations* (the hydrostatic Navier-Stokes equations applied to a perfect gas surrounding a rotating spherical planet) by means of spectral methods on horizontal levels (expanding the fields in terms of spherical harmonics) and with a finite-difference scheme in the vertical direction. For this study, data were taken from a MGCM run with spectral resolution T31 (jagged triangular truncation at total wavenumber 31). The vertical resolution is given by 25 unevenly spaced levels in terrain-following sigma coordinates ( $\sigma = p(x, y, z, t)/p_s(x, y, t)$ , where  $p_s$  is the surface pressure). The model includes parameterisation schemes of physical processes such as radiative transfer, surface and sub-surface processes, sub-grid scale dynamics and carbon dioxide condensation and sublimation (Forget *et al.*, 1999).

## 2 Vertical Modes and Energy Considerations

This study uses a *quasi-geostrophic approximation* (QG) to the dynamics of the atmosphere. This means that the leading order balance is between the Coriolis force and the horizontal pressure gradient: the so-called the *geostrophic balance*. This approximation is valid whenever the Rossby number

$$\text{Ro} \equiv \frac{U}{2\Omega a} \ll 1, \quad (1)$$

where  $U$  is a typical horizontal wind velocity,  $\Omega$  is the rotation rate of the planet and  $a$  is the planetary radius, giving the ratio between the inertia terms and the Coriolis force. The geostrophic approximation is useful for describing atmospheric motion for large-scale synoptic weather systems in extratropical latitudes. In the case of Mars, the horizontal wind reaches typical maximum speeds of  $U = 100$  m/s at a height of 30–50 km above the surface. Since the planetary radius of Mars is  $a = 3.394 \times 10^6$  m and its rotation rate is  $\Omega = 7.08822 \times 10^{-5} \text{ s}^{-1}$ , the maximum Rossby number is  $\text{Ro} = 0.2$ . We can therefore say that QG theory should be a reasonable approximation to large-scale motions, the case relevant to our work.

In the QG approximation we assume that the velocity can be divided into two parts

$$\mathbf{V} = \mathbf{V}_g + \mathbf{V}_a, \quad (2)$$

where the magnitude of the *ageostrophic wind velocity*  $\mathbf{V}_a$  is much smaller than that of the *geostrophic wind velocity*  $\mathbf{V}_g$ , the ratio being of the same order of magnitude as the Rossby number. Under these assumptions it is possible to derive a consistent set of equations describing the synoptic-scale atmospheric dynamical behaviour (Holton, 2004).

## 2.1 Vertical Structure Equation

One important result of QG theory is the conservation of *potential vorticity* for adiabatic flow. Using terrain-following sigma coordinates after linearisation, this conservation law may be expressed as

$$\frac{\partial}{\partial t} \left( \nabla^2 \psi + \left( \frac{f}{p_s} \right)^2 \frac{\partial}{\partial \sigma} \left( \frac{1}{S} \frac{\partial \psi}{\partial \sigma} \right) \right) + \frac{1}{\cos \phi} \frac{\partial \psi}{\partial \lambda} \frac{\partial f}{\partial \phi} = 0, \quad (3)$$

where  $\lambda$  and  $\phi$  are longitude and latitude, respectively,  $f \equiv 2\Omega \sin \phi$  is the Coriolis parameter, and  $S = S(\sigma)$  is the stratification parameter. The latter depends only on the vertical coordinate sigma and contains information about the vertical stratification of the atmosphere.  $\psi$  is the streamfunction and is related to the geostrophic wind velocity by the equation

$$\mathbf{V}_g = \mathbf{k} \times \nabla \psi, \quad (4)$$

where  $\mathbf{k}$  is a unit vector pointing upwards.

Assuming a separable solution of the form

$$\psi(\mathbf{x}, \sigma, t) = \tilde{\psi}(\mathbf{x}, t)H(\sigma), \quad (5)$$

where  $\mathbf{x}$  denotes the set of horizontal variables  $\{\phi, \lambda\}$  in spherical areographical coordinates, we obtain the equation for the vertical structure:

$$\frac{d}{d\sigma} \left( \frac{1}{S} \frac{dH}{d\sigma} \right) + \Lambda H = 0. \quad (6)$$

Here,  $\Lambda$  plays the role of an eigenvalue whose meaning will be fully discussed later. Equation (6) needs to be supplemented by suitable boundary conditions. These were chosen to be

$$\frac{dH}{d\sigma} = 0, \quad \text{at } \sigma = \sigma_1 \quad \text{and} \quad \sigma = 1, \quad (7)$$

where  $\sigma_1 = 4 \times 10^{-3}$  (approximately  $z = 73.7$  km) is the position of the upper boundary. The boundary conditions (7) imply the assumption of a rigid lid at the upper boundary,  $\sigma = \sigma_1$ . Physically, there is no lid at the top of the atmosphere and such an assumption may produce spurious free oscillations propagating vertically (Lindzen *et al.*, 1968). However, choosing homogeneous boundary conditions allows us to restrict the problem to the analysis of the lower and middle atmosphere, where most of the energy is found, and eliminates the upper atmosphere in a first approximation. It also makes our model consistent with the bounded MGCM.

The set of eigenfunctions  $\mathcal{H} = \{H_k(\sigma)\}$  for  $k = 0, 1, 2, \dots$ , constitute a complete orthogonal set since they are the eigenvectors of a self-adjoint operator and can be normalized by

$$\int_{\sigma_1}^1 H_k H_l d\sigma = \delta_{kl}. \quad (8)$$

## 2.2 Energy in the Vertical Modes

In order to investigate the energy distribution among the different vertical modes it is necessary to have suitable expressions for the energy content of each mode. There are basically two kinds of energy involved in the development of atmospheric processes. The first is *available potential energy* (APE), the fraction of the sum of the potential and internal energies in the atmosphere that is available for conversion into kinetic energy (Lorenz, 1955). It is the main source of energy for the maintenance of the general circulation at mid-latitudes and for the development of baroclinic waves. For the  $k$ -th vertical mode this is given by

$$A_k = \frac{f_0^2 a^2}{2g p_0} \Lambda_k \sum_{n,m} ' |(\tilde{\psi}_k)_n^m|^2, \quad (9)$$

where  $f_0$  and  $p_0$  are respectively the average of the Coriolis parameter and the surface pressure over the whole globe and  $g$  is the acceleration due to gravity.  $\Sigma'$  indicates that the term corresponding to  $n = 0$  is excluded from the sum.

The second kind of energy, *kinetic energy* (KE), associated with the squared velocity of the wind can be expressed for the  $k$ -th vertical mode as

$$K_k = \frac{p_0}{2g} \sum_{n,m} ' n(n+1) |(\tilde{\psi}_k)_n^m|^2. \quad (10)$$

The *total energy* (TE) in the  $k$ -th vertical mode is then defined as the sum of KE and APE in each mode. The ratio of KE to APE in the mode is proportional to  $\lambda_{Rk}^2 = p_0^2 / (f_0^2 \Lambda_k)$ , which is the square of the Rossby radius of deformation for the  $k$ -th vertical mode. It is a fundamental length scale in atmospheric physics and can be interpreted as ‘‘the horizontal scale at which rotation become as important as buoyancy effects’’ (Gill, 1982).

The relation between the Rossby radius of deformation and the eigenvalues of the vertical structure equation is now apparent since  $\Lambda_k$  is inversely proportional to  $\lambda_{Rk}^2$ . Figure 1 shows the Rossby radius of deformation for the first 21 vertical modes. Mode 0 is the *barotropic* mode. It corresponds to  $\Lambda = 0$  and is independent of height. The modes corresponding to  $k = 1, 2, \dots$ , are called the first *baroclinic* mode, second baroclinic mode, etc. The number  $k$  indicates the number of zeros which the mode has. Figure 2 shows

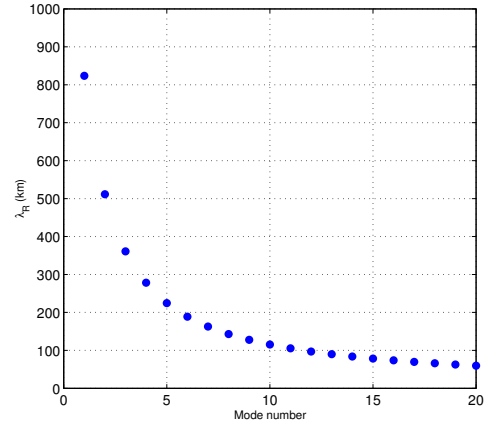


Figure 1. Rossby radius of deformation  $\lambda_{Rk}$  for  $k = 0, \dots, 20$ .

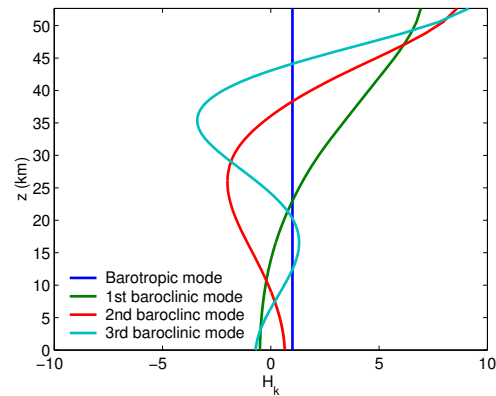


Figure 2. The vertical structure of the barotropic and the first three baroclinic modes.

the structure of the barotropic and the first three baroclinic modes. For the sake of clarity,  $z = -H \ln \sigma$  has been used as vertical coordinate with  $H = 10$  km taken as the proper scale height on Mars.

An important property of the vertical eigenmodes is the energy distribution. Figure 3 shows the KE, APE and TE content of the first 21 vertical modes. It also shows the fraction of the energy contained in the *zonal* (axisymmetric) flow and in the *eddies* (non-axisymmetric flow). KE decreases monotonically as the mode number increases. This is also the case for APE although there are four anomalies between the modes (6,7), (8,9), (14,15) and (19,20) where APE increases. This may be caused by the finite character of the time series under analysis. However, when looking at the distribution of TE (Figure 4) it is apparent that, despite these anomalies, most of the energy is found in the first few vertical modes so that it is necessary, for example, to keep only 12 modes including the barotropic one to retain 92.2% of the energy content in the whole atmosphere.

Figure 4 also shows that the fraction of energy contained in the eddies increases when more vertical modes are retained. This effect is mainly due to the distribution of APE since KE becomes negligible as

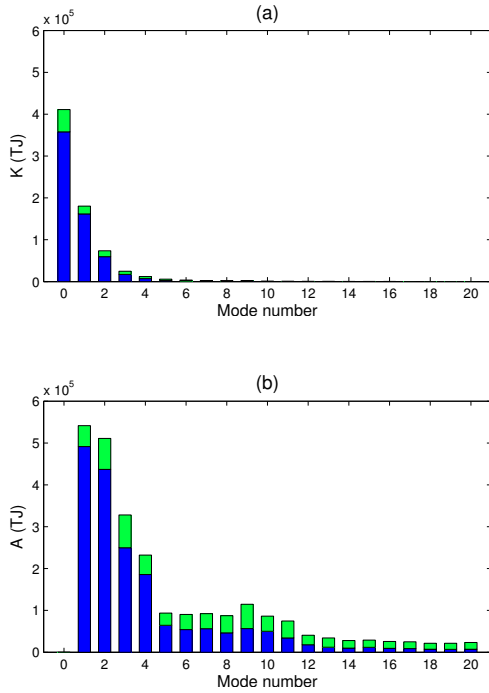


Figure 3. Distribution of the (a) kinetic energy,  $K$ , and (b) available potential energy,  $A$ , over the vertical modes and over the zonal (blue), and eddy (green) streamfunction fields.

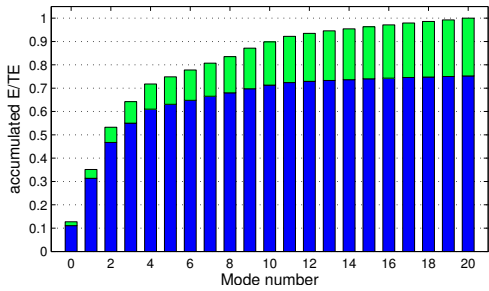


Figure 4. Accumulation of the total energy  $E_k = A_k + K_k$  over the vertical modes and over the zonal (blue), and eddy (green) streamfunction fields, normalized by the total energy contained by the whole atmosphere.

the mode number increases (Figure 3). It may also be caused by the interaction of higher order modes with topography, which is the main source of zonal asymmetry that is consistent with the structure of the vertical eigenmodes.

### 3 Proper Orthogonal Decomposition

The POD (Berkooz *et al.*, 1993; Holmes *et al.*, 1996) enables us to find a set of empirical orthogonal functions (EOFs). These optimise the variance of the system among all possible linear expansions and a given number of modes. By a suitable definition of the inner product, it is possible to use the same procedure to represent energy instead of variance and keep all the analysis in the spectral space.

### 3.1 Phase space

The streamfunction can be split into an axisymmetric zonal field  $\hat{\psi} = \hat{\psi}(\phi)$  and an eddy field  $\Psi = \Psi(\lambda, \phi, t)$ , and then expanded in terms of spherical harmonics  $Y_n^m = Y_n^m(\lambda, \phi)$  as:

$$\left. \begin{aligned} \hat{\psi} &= \sum_{n=0}^{N_0} \psi_n^0 Y_n^0 \\ \Psi &= 2\Re \left\{ \sum_{m=1}^{N-1} \sum_{n=m}^{N_m} \psi_n^m Y_n^m \right\} \end{aligned} \right\} \quad (11)$$

Note that in equation (11b) only the coefficients with positive  $m$  are used.

Equations (11) enable us to define two vector spaces on which to perform the POD separately: a real vector space formed by the real spectral coefficients of the zonal field,  $\psi_n^0$ , and a complex vector space formed by the complex spectral coefficients of the eddy field,  $\psi_n^m$ .

Let  $\psi_k \in \mathbb{V}^r$  (the  $k$ -th modal state vector with  $k = 0, \dots, \infty$ ) be defined as the column vector whose entries are determined by the spherical harmonic expansion of the  $k$ -th vertical mode  $\psi_k$ . Consider a jagged T31 resolution whose coefficients are ordered with increasing  $n$  within increasing  $m$ , taking first the coefficients for which the meridional wavenumber  $n - |m|$  is odd and then those for which it is even. Then

$$\psi_k = \begin{pmatrix} ((\tilde{\psi}_k)_n^m | n - m \text{ odd}) \\ ((\tilde{\psi}_k)_n^m | n - m \text{ even}) \end{pmatrix}, \quad (12)$$

where the inner parentheses also represent column vectors;  $m = 0$  in the case of the zonal field and  $m = 1, \dots, T_n - 1$  in the case of the eddy field while  $n = m, \dots, N_m$ .  $T_n = 31$  is the highest wavenumber in the expansion and  $N_m = 31$  if  $m$  is even and  $N_m = 30$  if  $m$  is odd.

The vector space  $\mathbb{V}^r$  is either  $\mathbb{R}^{31}$  or  $\mathbb{C}^{480}$  depending on the field that is being analysed, the former for the zonal field, the latter for the eddies.

Let the state vector, denoted by  $\psi = [\psi_0, \psi_1, \dots, \psi_q]^T \in \mathbb{V}^s$ , be the column vector of  $q + 1$  concatenated modal state vectors so that  $s = r(q + 1)$ , where  $r = 31$  for the zonal field and  $r = 480$  for the eddy field. The number  $q + 1$  of vertical modes varies according to the amount of energy of the original system to be explained. For instance, to explain 77.8 % of the total available energy it is sufficient to retain the barotropic and the first six baroclinic modes, while to represent 92.2 % of the total available energy it is necessary to use at least the first 11 baroclinic modes in addition to the barotropic mode (See figure 4). The complex space of  $s$  dimensions, where the state vector evolves, constitutes the phase space of interest.

It is also possible to perform the decomposition on the complete streamfunction field using real principal components (Schubert, 1985). However, this formulation requires almost four times as much computer memory

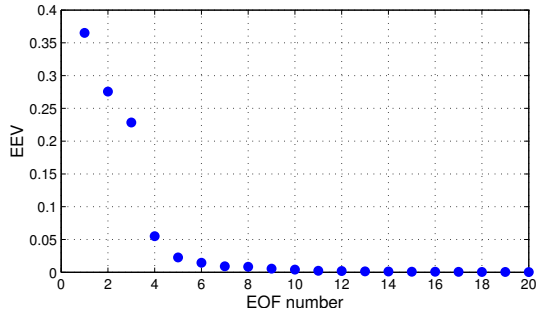


Figure 5. Empirical eigenvalues  $\lambda$  corresponding to the zonal flow. The eigenvalues are normalized so that their sum is equal to unity.

as the method presented here since it employs not only the spectral coefficients with  $m \geq 0$  but the complete set of coefficients.

### 3.2 Metric of the Phase Space

To give a metric to our vector space it is necessary to define an inner product. Whitehouse (2004a,b) concluded that of the three norms that they tested (correlation, KE and TE) the best representation was obtained with the TE norm. Achatz and Opsteegh (2003a,b) also used the TE norm in order to retain interactions between the velocity and temperature fields. We, therefore, adopt the same norm in this work.

We define the energy matrix of the  $k$ -th mode as

$$\mathbf{E}_k = C \frac{p_0}{2g} \text{diag} \left( \left( \frac{a}{\lambda R k} \right)^2 + n(n+1) \right), \quad (13)$$

where constant  $C$  takes the value  $C = 1$  for the zonal motion and  $C = 2$  for the eddy field.

The total energy matrix  $\mathbf{E}$  is constructed as a block diagonal matrix whose entries are the energy matrices  $\mathbf{E}_k$ , i.e.

$$\mathbf{E} = \text{diag} (\mathbf{E}_0, \dots, \mathbf{E}_q). \quad (14)$$

We define the inner product in  $\mathbb{V}^s$  as

$$(\mathbf{u}, \mathbf{v}) = \mathbf{u}^\dagger \mathbf{E} \mathbf{v}, \quad (15)$$

where  $\mathbf{u}, \mathbf{v} \in \mathbb{V}^s$  are two arbitrary state vectors and  $\mathbf{u}^\dagger$  denotes the conjugate transpose of  $\mathbf{u}$ . Clearly  $\mathbf{u}^\dagger = \mathbf{u}^T$  in the case of  $\mathbb{R}^s$ , where  $\mathbf{u}^T$  is the transpose of  $\mathbf{u}$ .

The inner product must satisfy the usual properties of a Hermitian inner product. In particular,  $(\mathbf{u}, \mathbf{v}) = (\mathbf{v}, \mathbf{u})^*$ , where  $z^*$  is the complex conjugate of  $z \in \mathbb{C}$ . Since  $\mathbf{E}$  is a positive definite matrix

$$\|\mathbf{u}\| = (\mathbf{u}, \mathbf{u})^{1/2} \geq 0 \quad (16)$$

with the equality holding only if  $\mathbf{u} = \mathbf{0}$ . With this definition the energy is given by the squared norm of

Table 1. Energy content of the first ten zonal and eddy eigenmodes. (AZE = accumulated zonal energy; AEE = accumulated eddy energy)

Mode	Zonal (%)	AZE (%)	Eddy (%)	AEE (%)
1	36.51	36.51	47.56	47.56
2	27.57	64.08	26.50	74.06
3	22.85	86.93	3.03	82.52
4	5.50	92.42	2.28	85.55
5	2.26	94.69	1.20	87.83
6	1.45	96.14	1.00	89.03
7	0.91	97.05	0.92	90.03
8	0.83	97.88	0.77	90.95
9	0.55	98.43	0.66	91.72
10	0.40	98.83	0.57	92.39

the state vector, i.e.

$$E = (\boldsymbol{\psi}, \boldsymbol{\psi}) = \|\boldsymbol{\psi}\|^2. \quad (17)$$

We adopt the procedure of Holmes *et al.* (1996) to derive the EOFs. Following Selten (1993) and Whitehouse *et al.* (2004a), the mean state is retained so that dynamical interactions between it and the EOFs are allowed. Energy rather than variance is optimized.

Let  $\mathcal{S} = \{\boldsymbol{\psi}(t) | \boldsymbol{\psi}(t) \in \mathbb{V}^s\}$  be a set of realizations of the vector  $\boldsymbol{\psi}$ . Suppose that we want to find a basis  $\{\boldsymbol{\phi}_j\}_{j=1}^s$  spanning  $\mathbb{V}^s$ . The finite-dimensional expansion

$$\boldsymbol{\psi}^N(t) = \sum_{j=1}^N a_j(t) \boldsymbol{\phi}_j, \quad (18)$$

explains more of the energy contained in  $\boldsymbol{\psi} \in \mathbb{V}^s$  than any other linear expansion of the same dimension  $N$ . To do this we find  $\boldsymbol{\phi}$  satisfying

$$\max_{\boldsymbol{\phi} \in \mathbb{V}^s} \frac{\langle |(\boldsymbol{\psi}, \boldsymbol{\phi})|^2 \rangle}{\|\boldsymbol{\phi}\|^2}, \quad (19)$$

where  $|\cdot|$  denotes the modulus. This can be done using standard calculus of variations techniques (not reproduced here) to obtain

$$\langle \boldsymbol{\psi} \boldsymbol{\psi}^\dagger \rangle \mathbf{E} \boldsymbol{\phi} = \lambda \boldsymbol{\phi}. \quad (20)$$

The required basis is constituted from eigenvectors of the autocorrelation matrix  $\mathbf{C} = \langle \boldsymbol{\psi} \boldsymbol{\psi}^\dagger \rangle$  post-multiplied

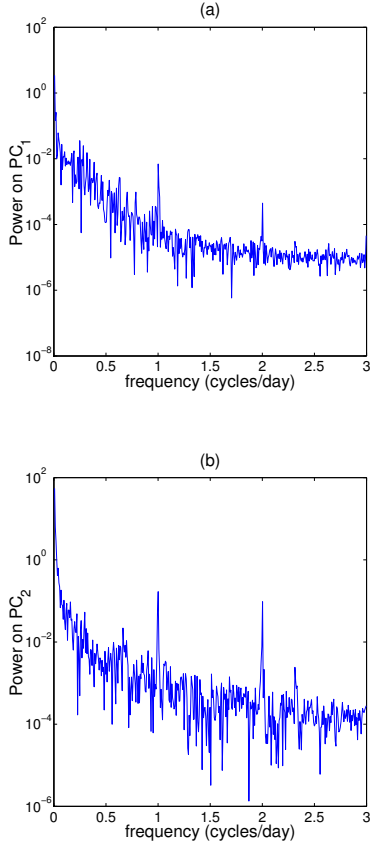


Figure 6. Power spectra of (a) the first, and (b) second zonal PCs, showing the relative importance of the diurnal and semidiurnal cycles as well as of processes of low frequency (long period).

by the TE matrix  $\mathbf{E}$ . While  $\mathbf{C}$  is Hermitian and  $\mathbf{E}$  is diagonal with real entries, the matrix product  $\mathbf{C}\mathbf{E}$  is neither Hermitian nor diagonal. However, by defining  $\mathbf{D} \equiv \mathbf{E}^{1/2}\mathbf{C}\mathbf{E}^{1/2}$  where  $\mathbf{E} \equiv \mathbf{E}^{1/2}\mathbf{E}^{1/2}$  we can write (Whitehouse *et al.*, 2004a)

$$\mathbf{D}\boldsymbol{\theta} = \lambda\boldsymbol{\theta}, \quad (21)$$

where  $\boldsymbol{\theta} \equiv \mathbf{E}^{1/2}\boldsymbol{\phi}$ . This ensures that the eigenvalues  $\lambda$  are real (since  $\mathbf{D}$  is Hermitian by definition) and that the eigenvectors  $\boldsymbol{\theta}_i$  are orthogonal under the usual inner product, i.e.

$$\boldsymbol{\theta}_i^\dagger \boldsymbol{\theta}_j = \left(\mathbf{E}^{1/2}\boldsymbol{\phi}_i\right)^\dagger \left(\mathbf{E}^{1/2}\boldsymbol{\phi}_j\right) = \boldsymbol{\phi}_i^\dagger \mathbf{E}\boldsymbol{\phi}_j. \quad (22)$$

Therefore, the empirical eigenvectors are orthonormal under the inner product defined by  $\mathbf{E}$ .

The set  $\{\boldsymbol{\phi}_j\}$  is the required basis and can, therefore, be used to expand the original vector  $\boldsymbol{\psi}_k$

$$\boldsymbol{\psi}_k(t) = \sum_{j=1}^{\infty} a_j(t)\boldsymbol{\phi}_j^k. \quad (23)$$

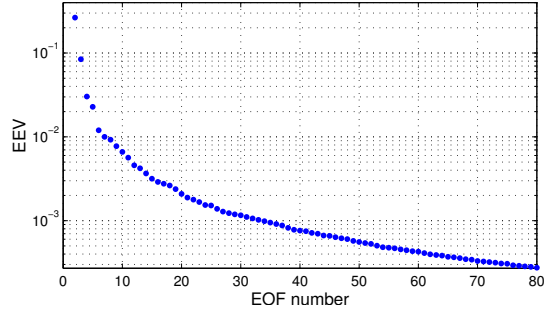


Figure 7. Empirical eigenvalues corresponding to the eddies. The eigenvalues are normalized so that their sum is equal to unity.

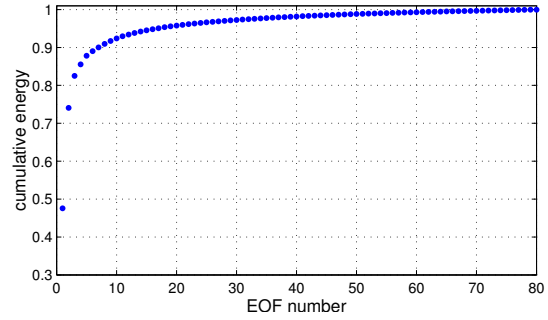


Figure 8. Accumulation of the energy throughout the eddy EOFs.

The time-dependent coefficients  $\{a_j(t)\} \in \mathbb{V}$ , can be calculated in the usual way by using the orthonormality of the empirical eigenvectors to obtain  $a_j(t) = (\boldsymbol{\phi}_j, \boldsymbol{\psi})$ . The coefficients  $a_j$  are called Principal Components (PC) and can be either real or complex depending on whether the zonal or the eddy field is being considered.

To return to physical space, we replace  $\{\boldsymbol{\theta}_j\}_{j=1}^{\infty}$  by  $\{\boldsymbol{\phi}_j\}_{j=1}^{\infty}$  using the equation  $\boldsymbol{\phi}_j = \mathbf{E}^{-1/2}\boldsymbol{\theta}_j$ . Note that the decomposition has been carried out on only a half of the  $(n, m)$ -space, where  $m \geq 0$  and so, to recover the streamfunction field on a longitude-latitude grid, equations (11) must be used.

### 3.3 Zonal Field Decomposition

The POD was carried out using  $q = 11$  baroclinic modes and the barotropic mode. This represents 92.2% of the total energy of the original system (c.f. Figure 4).

Figure 5 shows the set of empirical eigenvalues (EEVs) of the zonal field suitably normalized so that their sum is equal to unity. The figure shows the relative significance of the first three modes, which together contain 86.93% of the total energy in the zonal field and approximately 80.1% of the total energy in the original system. The fourth mode contains 5.50% of the zonal energy while the fifth contains 2.26%. The subsequent modes each contain less than 2% (see Table 1). Virtually, 100% of the zonal energy is achieved within 26 modes.

The evolution of the PCs is mainly dominated by the

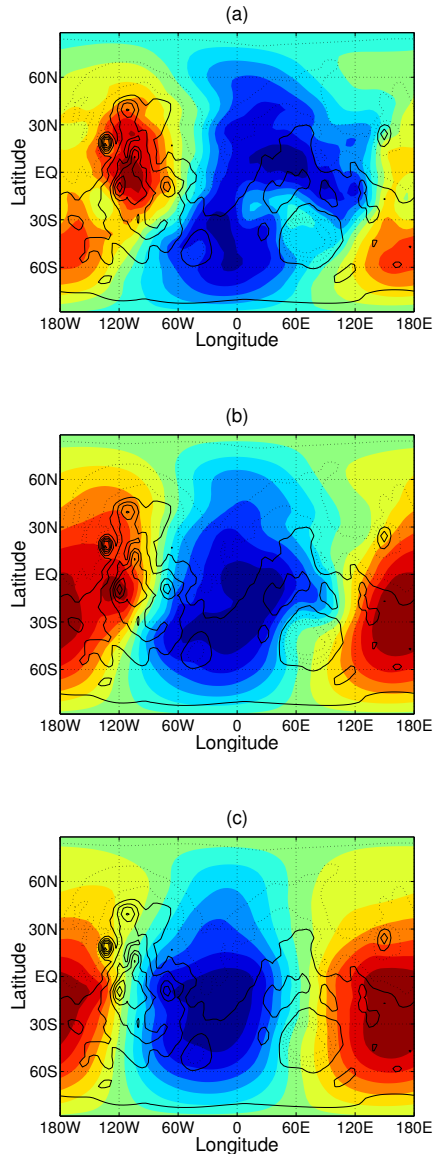


Figure 9. First eddy EOF after transforming to physical grid at approximate heights (a)  $z = 5$  km, (b)  $z = 10$  km, and (c)  $z = 20$  km. The approximate height  $z$  has been calculated using  $z = -H \ln \sigma$ , where  $H = 10$  km was taken as the proper scale height on Mars.

seasonal cycle. However, the diurnal and semi-diurnal tides are also important as can be seen from the power spectra (Figure 6) where the significance of frequencies corresponding to periods of 1 sol and 0.5 sol is shown. It is apparent that periodic components in the time series corresponding to periods longer than 1 sol are also important.

### 3.4 Eddy Field Decomposition

The decomposition of the eddy field yields the set of eigenvalues shown in Figure 7 while the accumulation of energy throughout the modes is shown in Figure 8. The first EOF contains 47.56% of the eddy energy, while the second contains 26.50% (See Table 1). In

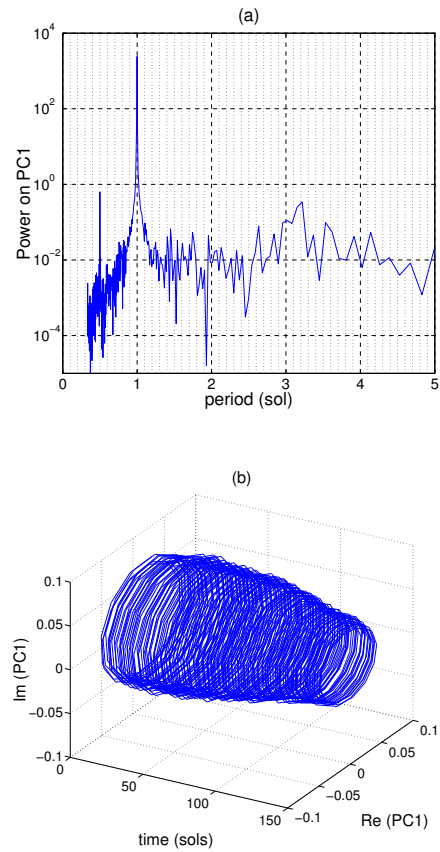


Figure 10. (a) Power spectrum and (b) evolution in the complex plane of PC1. The regularity of this mode is due to the strong influence of the diurnal cycle over it which leads to the development of thermal tides traveling westwards.

this case the energy is distributed among more modes so that to account for 90% of the TE, seven modes are required whereas seventeen modes are needed to explain 95% of the TE. In this paper we shall focus on the behaviour of the first (the most energetic) and the third eddy EOFs to illustrate the use of the POD to analyse baroclinic waves on Mars.

The PCs associated with the eddy streamfunction field are complex quantities in general and can be written as

$$a_j(t) = A_j(t)e^{iS_j(t)}, \quad (24)$$

where  $A_j$  is the amplitude and  $S_j$  is the phase of the  $j$ -th PC. This associates two real functions, the real and the imaginary parts of each PC, with each mode.

The state vector can be written in terms of EOFs by substituting equation (24) into (23). Recalling that the entries of the state vector are spectral coefficients of vertical modes, a single vertical mode can be written as

$$\Psi = 2\Re \left\{ \sum_j \sum_{n,m} A_j C_n^m \Phi_n^m P_n^m e^{m\lambda + S_j} \right\}, \quad (25)$$

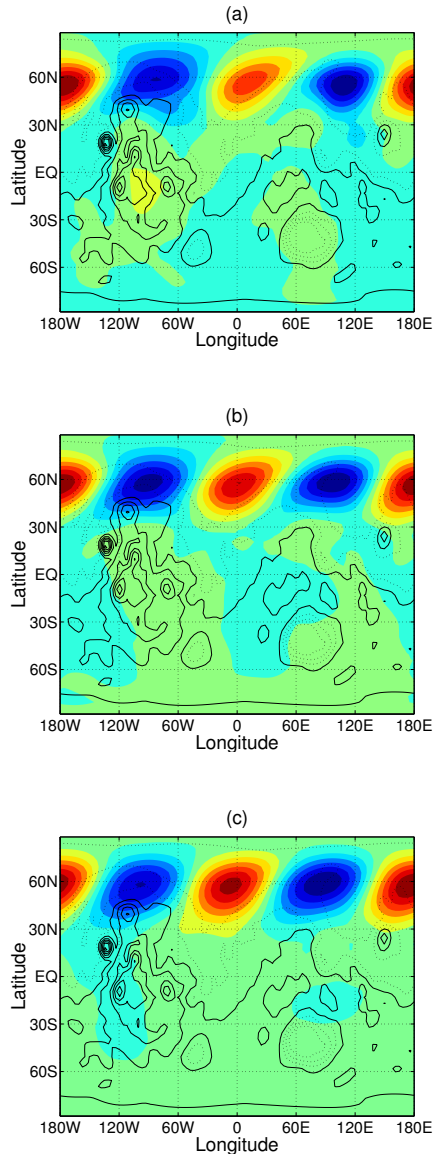


Figure 11. Third eddy EOF after transforming to physical grid at approximately (a)  $z = 5$  km, (b)  $z = 10$  km, and (c)  $z = 20$  km. The approximate height  $z$  has been calculated using  $z = -H \ln \sigma$ , where  $H = 10$  km was taken as the proper scale height on Mars.

where  $C_n^m$  are simply the normalization coefficients of the spherical harmonics. Note that the subscript  $k$  and the tilde indicating the vertical mode were omitted for the sake of clarity in notation. Since  $m > 0$ ,  $\dot{S}_j > 0$  indicates westward whereas  $\dot{S}_j < 0$  indicates eastward propagation, where  $\dot{S}$  is the time derivative of  $S$ .

The most energetic EOF (Figure 9) is composed of a diurnal tide of longitudinal wavenumber one and of period 1 sol traveling westwards since  $\dot{S}_1 = 2\pi > 0$ . The power spectrum (Figure 10a) confirms the dominance on this mode of the diurnal tide. The power spectrum also shows the presence of a much weaker signal with a period of 0.5 sol which indicates the influence of the semi-diurnal tide on this EOF. While the intensity

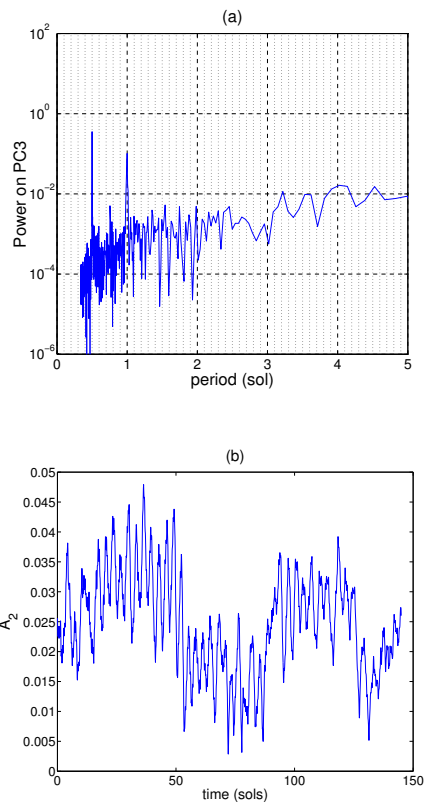


Figure 12. (a) Power spectrum and (b) evolution in the complex plane of PC3. The main characteristic of this mode is the presence of a vacillating baroclinic wave traveling eastwards over the northern hemisphere.

of PC1 (PC corresponding to mode 1) is nearly constant (Figure 10b), the influence of the seasonal cycle is apparent. As expected, the influence of topography causes a distortion of the waves near the surface but this effect is attenuated as height increases. The influence of topography over the atmospheric dynamics is also important for the second EOF. It represents stationary waves trapped by orographic structures oscillating with period 1 sol.

The third EOF is composed of a baroclinic wave travelling eastwards (since  $\dot{S} \simeq -5\pi/8 < 0$ ) with longitudinal wavenumber two and period  $\tau = 3.2$  sols. The centre of the wave is located around  $60^\circ\text{N}$  at every height level (Figure 11). One characteristic of a baroclinic wave is that the geopotential trough and ridge axes slope westwards with height (see, for instance, (Holton, 2004)). This provides confirmation of the character of the wave under analysis. An interesting feature of this EOF is the evidence of amplitude vacillation with a vacillation period of around 100 sols (Figure 12b). A better measure of the vacillation period would require original data for a whole year or for several years. The influence of the semi-diurnal tide is more significant than the diurnal one for the third EOF, although the latter is still apparent (Figure 12a).

#### 4 Conclusion

In this paper a time series of the evolution of the streamfunction on Mars, generated by the MGCM, was decomposed into vertical and horizontal modes. The selected run corresponds to the transition between autumn and winter in the Martian northern hemisphere when the baroclinic activity is stronger.

By means of the vertical decomposition it was possible to find and retain the most energetic modes, discarding the rest. For example in order to represent 92.2% of the TE in the original system we required 12 vertical modes.

The POD analysis was carried out on the zonal (axisymmetric) part of the streamfunction and on the eddy part separately so that complex PCs could describe the evolution of the eddy field. This formulation has the advantage of using less computer memory, a fact that becomes important when working with high spectral resolution models. One drawback, however, is that two state variables are required for each mode when constructing low-order models via Galerkin approximation.

The zonal field analysis showed that the first four EOFs contain more than 90% of the TE, while to achieve the same level of accuracy in the eddy field, at least 7 EOFs are required. For the eddy field, an example involving the first and the third EOFs was given. The first EOF, containing 47.56% of the energy in the eddy field, is strongly affected by the diurnal cycle. This mode consisted basically of a wave of wavenumber one and period one sol traveling westwards which corresponds to a thermal tide. The third EOF, containing 3% of the energy in the eddy field, consisted of a wave with the characteristics of a baroclinic wave with the trough and ridge streamfunction axes tilting westwards with height. This EOF corresponds to a wavenumber two traveling eastwards with a period 3.2 sols. The evolution of the corresponding PC showed the vacillation of the baroclinic wave.

The analysis reported in this paper therefore gives an indication of the feasibility of constructing low-order models of the dynamical behaviour of the Martian atmosphere by representing a large amount of the original system's TE in terms of a few vertical and horizontal modes. In the case discussed here, for example, 12 vertical modes and 30 eddy EOFs (containing 97% of the TE in the eddy field) would be useful to represent 89% of the TE in the original system.

#### Acknowledgements

OMA would like to thank the National Council of Science and Technology of Mexico (CONACYT) for the grant awarded.

#### References

Achatz, U. and G. Branstator (1999). A two-layer model with empirical linear corrections and reduced

order for studies of internal climate variability. *J. Atmos. Sci.* **56**, 3140–3160.

Achatz, U. and J.D. Opsteegh (2003a). Primitive-equation-based low-order models with seasonal cycle. Part I: Model construction. *J. Atmos. Sci.* **60**(3), 465–477.

Achatz, U. and J.D. Opsteegh (2003b). Primitive-equation-based low-order models with seasonal cycle. Part II: Application to complexity and nonlinearity of large-scale atmospheric dynamics. *J. Atmos. Sci.* **60**(3), 478–490.

Berkooz, G., P. Holmes and J.L. Lumley (1993). The proper orthogonal decomposition in the analysis of turbulent flows. *Annu. Rev. Fluid Mech.* **25**, 539–575.

Collins, M., S.R. Lewis, P.L. Read and F. Hourdin (1996). Baroclinic wave transitions in the martian atmosphere. *Icarus* **120**, 344–357.

Forget, F., F. Hourdin, R. Fournier, C. Hourdin, O. Talagrand, M. Collins, S.R. Lewis and P.L. Read (1999). Improved general circulation models of the martian atmosphere from the surface to above 80 km. *J. Geophys. Res. Planet* **104**(10), 24155–24176.

Gill, A.E. (1982). *Atmosphere-ocean dynamics*. Vol. 30 of *International Geophysical Series*. Academic Press.

Holmes, P., J.L. Lumley and G. Berkooz (1996). *Turbulence, coherent structures, dynamical systems, and symmetry*. Cambridge monographs on mechanics. Cambridge University Press.

Holton, J.R. (2004). *An introduction to dynamic meteorology*. Vol. 88 of *International Geophysics Series*. 4th ed.. Elsevier Academic Press.

Kwasniok, F. (2004). Empirical low-order models of barotropic flow. *J. Atmos. Sci.* **61**, 235–245.

Lindzen, R.S., E.S. Batten and J.W. Kim (1968). Oscillation in atmospheres with tops. *Mon. Weath. Rev.* **96**(3), 133–140.

Lorenz, E.N. (1955). Available potential energy and the maintenance of the general circulation. *Tellus* **7**(2), 157–167.

Read, P. L. and S.R. Lewis (2004). *The Martian climate revisited*. Springer-Praxis books in geophysical sciences. Springer-Praxis.

Schubert, S.D. (1985). A statistical-dynamical study of empirically determined modes of atmospheric variability. *J. Atmos. Sci.* **42**(1), 3–17.

Selten, F.M (1993). Toward an optimal description of atmospheric flow. *J. Atmos. Sci.* **50**(6), 861–877.

Whitehouse, S.G., S.R. Lewis, I.M. Moroz and P.L. Read (2004a). A simplified model of the Martian atmosphere. Part 1: a diagnostic analysis. *Nonlinear Proc. Geophys.* Submitted.

Whitehouse, S.G., S.R. Lewis, I.M. Moroz and P.L. Read (2004b). A simplified model of the Martian atmosphere. Part 2: a POD-Galerkin analysis. *Nonlinear Proc. Geophys.* Submitted.